Data-Driven Sparse Model Identification of Inverter-Based Resources for Control in Smart Grids

1st Javad Khazaei
Electrical and Computer Engineering
Lehigh University
Middletown, PA, U.S.
khazaei@lehigh.edu

2nd Wenxin Liu
Electrical and Computer Engineering
Lehigh University
Bethlehem, U.S.
wel814@lehigh.edu

2nd Faegheh Moazeni
Civil and Environmental Engineering
Lehigh University
Bethlehem, PA , U.S.
moazeni@lehigh.edu

***Abstract*—With the growing complexity of inverter-dominated grids, there is an emerging need for developing effective modeling tools to identify the dynamics of inverter-based resources (IBRs) interconnected to the grid. This paper utilizes a data-driven approach for identifying the dynamics of grid-tie IBRs in modern power systems. By leveraging the available measurements of the grid-tie IBR and estimation of derivatives of the states, sparse identification of nonlinear dynamics (SINDy) is utilized to obtain the IBR dynamics by selecting a library of candidate functions. The obtained data-driven model is then utilized for designing controllers to regulate the active and reactive powers of the grid-tie IBR. Time-domain simulations validate the effectiveness of the proposed data-driven model identification approach for control purposes in smart grids.**

***Keywords*—** Distributed Energy Resources, Sparse Identification, Koopman Theory, Data-driven System Identification.

I. Introduction

In an effort reducing the carbon emissions in electricity grid, renewable energy resources are widely being integrated into the grid [1]–[6]. The governing equations of these inverter-based resources (IBRs) in smart grids is a critical step in the modeling and control of these distributed energy resources (DERs) for guaranteed stability of the grid. Data-driven modeling of smart grid assets is currently undergoing a revolution due to the availability of high-resolution measurements from field devices.

System identification tools comprise a large collection of approaches that can be utilized to characterize dynamics from data. Many approaches have been utilized for data-driven model identification of dynamics including dynamic mode decomposition (DMD) [7], [8], neural networks (NNs) [9], [10], Koopman operator [11], [12], and sparse identification of nonlinear dynamics (SINDy) [13], [14]. In power system area, several recent studies have focused on data-driven modeling using these approaches [15]–[20]. For example, dynamic mode decomposition was utilized in [15] for microgrid control that is delay tolerant, or Koopman operator was utilized in [17] to identify the dynamics of generators for state-estimation purposes. As another example, a data-driven approach using machine learning tools was proposed in [19] to identify the lifetime of lithium-ion batteries.

Among these methods, dynamic mode decomposition heavily relies on a linear dynamics assumption but can handle high-dimensional data. Neural network-based approaches require a large amount of training data and are not interpretable [13], [14]. Koopman operator connects dynamic mode decomposition to nonlinear dynamics through an infinite dimensional linear operator also known as Koopman operator. Under special circumstances and provided that a good measurement basis is selected, Koopman operator may converge to a finite dimensional space, but it is not guaranteed for many systems [11], [12]. Sparse identification uses the sparse regression technique to identify dominant dynamics of candidate functions, and has shown promise in accurately modeling the unknown dynamics of nonlinear systems [21], [22]. Among the major advantages of SINDy is the sparsity approach which is easy to implement, reduces the training time, is interpretable, and provides an accurate formulation that outperforms other model identification techniques. While the existing research shows the significant potential of SINDy for identifying nonlinear dynamics of dynamical systems, their application for DER control have not been reported yet.

To address the existing knowledge gaps for identifying DER dynamics in smart grids, this paper investigates the application of sparse identification theory for control purposes in smart grids. Using sparse identification, dynamics of DERs will be identified using measurements. The learned nonlinear dynamics can then be used control purposes. Such control framework can significantly reduce the complexities of existing IBR control designs that heavily rely on physics-based models.

The rest of the paper is organized as follows: Section II formulates the IBR dynamics. Sparse identification of IBR dynamics is included in Section III. Time-domain validations are included in Section IV and Section V concludes the paper.

II. Problem Formulation

Fig. 1 depicts an IBR that is connected to the main grid through point of common coupling (PCC). The IBR is composed of the energy source (i.e., solar, wind, storage), a voltage source converter (VSC), and an LCL filter. In this

This research was in part under support from the National Science Foundation under Grant NSF-EPCN 2221784. The authors are with the college of Engineering at Lehigh University, Bethlehem, PA 18015 USA.

figure, L_c and r_c, and C_f are the inverter filtering components, and L_g, r_g are the grid impedance components.

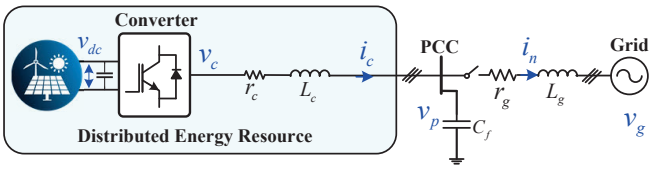

Figure. 1 Schematic of a grid-tie IBR.

A. AC-side Dynamics

Referring to Fig. 1, dynamics of the system in dq frame can be expressed as:

$$v_{cd} - v_{pd} + \omega_0 L_c i_{cq} = (L_c s + r_c) i_{cd} \quad (1)$$
$$v_{cq} - v_{pq} - \omega_0 L_c i_{cd} = (L_c s + r_c) i_{cq} \quad (2)$$
$$v_{pd} - v_{gd} + \omega_0 L_n i_{nq} = (L_n s + r_n) i_{nd} \quad (3)$$
$$v_{pq} - v_{gq} - \omega_0 L_n i_{nd} = (L_n s + r_n) i_{nq} \quad (4)$$
$$i_{cd} - i_{nd} + \omega_0 C_f v_{pq} = C_f s v_{pd} \quad (5)$$
$$i_{cq} - i_{nq} - \omega_0 C_f v_{pd} = C_f s v_{pq} \quad (6)$$

where $s = \dfrac{d}{dt}$ is the Laplace operator, ω_0 is the nominal frequency of the system, i.e., 377 rad/s, v_{cd}, v_{cq}, i_{cd}, and i_{cq} are the dq-frame components of the converter output voltage and current, respectively. Also, v_{pd}, v_{pq}, v_{gd}, and v_{gq} are the dq-frame components of the voltage at the PCC and grid, respectively, and i_{nd} and i_{nq} are the dq-frame components of the grid current. The above equation can be written in the following state space form:

$$\begin{bmatrix} \dot{i}_{cd} \\ \dot{i}_{cq} \\ \dot{v}_{pd} \\ \dot{v}_{pq} \\ \dot{i}_{nd} \\ \dot{i}_{nq} \end{bmatrix} = \begin{bmatrix} -\frac{r_c}{L_c} & \omega_0 & 0 & 0 & -\frac{1}{L_c} & 0 \\ -\omega_0 & -\frac{r_c}{L_c} & 0 & 0 & 0 & -\frac{1}{L_c} \\ 0 & 0 & -\frac{r_g}{L_g} & \omega_0 & \frac{1}{L_g} & 0 \\ 0 & 0 & -\omega_0 & -\frac{r_g}{L_g} & 0 & \frac{1}{L_g} \\ \frac{1}{C_f} & 0 & -\frac{1}{C_f} & 0 & 0 & \omega_0 \\ 0 & \frac{1}{C_f} & 0 & -\frac{1}{C_f} & -\omega_0 & 0 \end{bmatrix} \begin{bmatrix} i_{cd} \\ i_{cq} \\ v_{pd} \\ v_{pq} \\ i_{nd} \\ i_{nq} \end{bmatrix} + g(u)$$

$$g(u) = \begin{bmatrix} \frac{v_{cd}}{L_c} & \frac{v_{cq}}{L_c} & 0 & 0 & \frac{-v_{gd}}{L_g} & \frac{-v_{gq}}{L_g} \end{bmatrix}^T. \quad (7)$$

B. Inner Current Controller

In the VSC, the inner current controller generates the reference voltages in the dq-frame, which are fed to the pulse width modulation (PWM) generation unit. Dynamics of the inner current control loop in the dq frame can be represented as:

$$v_{cd}^* = \left(k_{pi} + \frac{k_{ii}}{s}\right)(i_{cd}^* - i_{cd}) - \omega L_f i_{cq} + v_{pd},$$
$$v_{cq}^* = \left(k_{pi} + \frac{k_{ii}}{s}\right)(i_{cq}^* - i_{cq}) + \omega L_f i_{cd} + v_{pq}. \quad (8)$$

where v_{cd}^* and v_{cq}^* are the reference voltages of the convert in dq frame, i_d^* and i_q^* are the reference currents generated by the outer control loop, i_{1d} and i_{1q} are the currents measured at the PCC and the feed forward voltage components, v_{pd} and v_{pq}, are measured at the PCC. Furthermore, k_{pi} and k_{ii} are the PI controller gains for the inner current loop controller.

C. Active and Reactive Power Controller

Assuming that a phase-locked loop is implemented that can synchronize the converter to the grid by forcing the q component of the PCC voltage to zero referring to [23], the outer loops of the IBR can directly control the active and reactive powers, P, Q, delivered to the grid. Two proportional controllers generate the reference currents (i_d^* and i_q^*) using:

$$i_{cd}^* = \frac{2}{3v_{pd}} P^*,$$
$$i_{cq}^* = -\frac{2}{3v_{pd}} Q^*. \quad (9)$$

The outer control loop dynamics in the dq-frame are expressed in (9), where P^* and Q^* are active and reactive power demanded by the grid, P and Q are active and reactive power measured at the PCC, which can be calculated using $P = 1.5(v_{pd} i_{cd} + v_{pq} i_{cq})$, $Q = 1.5(-v_{pd} i_{cq} + v_{pq} i_{cd})$ [23].

D. Data-Driven Model Identification

In the absence of detailed information about DERs and their converter parameters, the objective is to identify the lumped dynamic model of DERs in equation (7) from available measurements of the states. We will utilize sparse identification of nonlinear dynamics (SINDy) to identify the dynamics from measurements and utilize the data-driven model to design a controller that regulates the active and reactive power of the IBRs. An overview of the proposed approach for data-driven model identification and control of DERs using SINDy is depicted in Figure. 2. By perturbing the input (converter voltage) and collecting enough measurement samples, sparse regression can be utilized to identify the nonlinear dynamics by selecting a good library of candidate functions. The identified data-driven model can then be used for control design purposes. The control design includes the inner current control loop that regulates the converter current through proportional integral (PI) regulators and the outer loop regulates the active and reactive powers of the converter in grid-tie mode of operation.

III. Model-Free Identification of DERs

The sparsity promoting techniques are commonly used to identify the candidate functions with the greatest impact on the dynamics of dynamical systems containing few nonlinear terms. Originally proposed in [21], SINDy utilizes a symbolic regression technique to identify the system dynamics. The sparse identification is based on the fact that many dynamical systems with the form $\dot{\mathbf{x}} = \mathrm{f}(\mathbf{x}, \mathbf{u})$ have very few terms on the right. Considering the physical dynamics of a DER is represented by $\dot{\mathbf{x}} = \mathbf{f}(\mathbf{x}) + \mathbf{g}(\mathbf{x})\mathbf{u}$, where $\mathbf{x}(t) \in \mathbb{R}^n$ is the

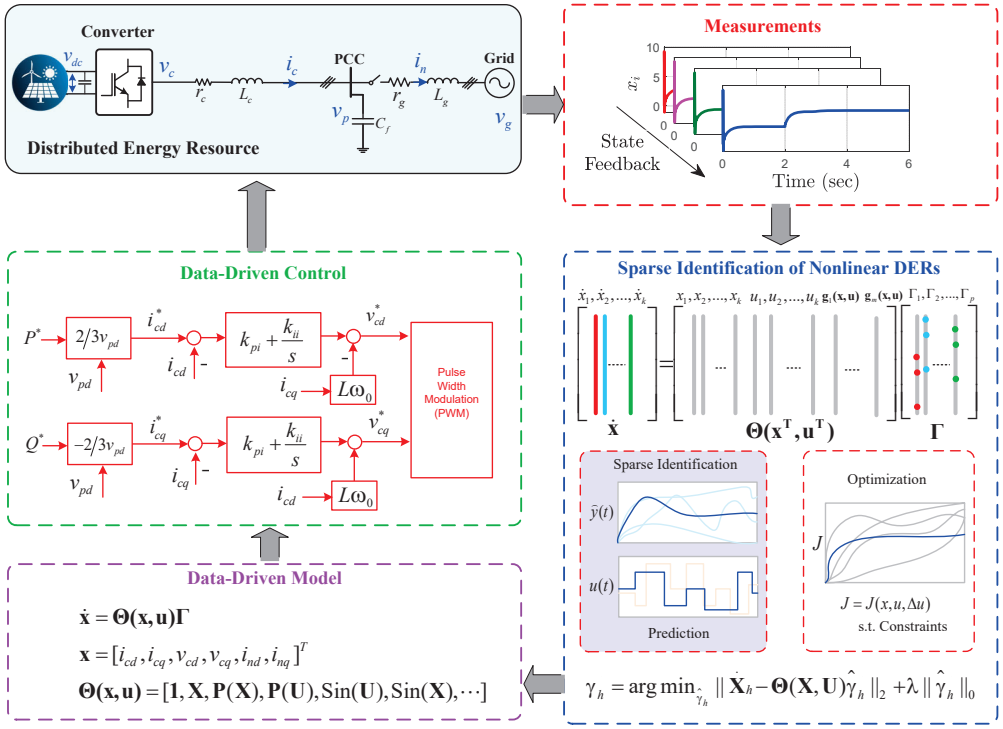

Figure. 2 Identified DER dynamics using SINDy.

state vector, $\mathbf{u}(t) \in \mathbb{R}^q$ is the input or control vector, and $\mathbf{f}(\mathbf{x}(t), \mathbf{u}(t)) : \mathbb{R}^n \times \mathbb{R}^q \to \mathbb{R}^n$, the objective is to reconstruct (7) from data. The process is explained in below.

A. Data Collection

The first step involves collecting m samples of data from the states and inputs by collecting a time-history of the state vector $\mathbf{x}(t)$, input $\mathbf{u}(t)$, and $\dot{\mathbf{x}}(t)$. The measurement data is sampled at m intervals $t_1,\ t_2,\ \ldots,\ t_m$ and is arranged into a matrix $\mathbf{X} \in \mathbb{R}^{n \times m}$,

$$\mathbf{X} = \begin{bmatrix} | & | & & | \\ \mathbf{x}(t_1) & \mathbf{x}(t_2) & \ldots & \mathbf{x}(t_m) \\ | & | & & | \end{bmatrix} \tag{10}$$

and inputs for t_m samples are written into a matrix $\mathbf{U} \in \mathbb{R}^{n \times m}$,

$$\mathbf{U} = \begin{bmatrix} | & | & & | \\ \mathbf{u}(t_1) & \mathbf{u}(t_2) & \ldots & \mathbf{u}(t_m) \\ | & | & & | \end{bmatrix} \tag{11}$$

since in most practical systems the derivative measurements are not observable, the measurements for derivatives can be approximated numerically from $\mathbf{X}$.

B. Estimating the Derivatives, $\dot{\mathbf{X}}$

A difference approximation is used to solve ordinary and partial differential equations numerically. If a smooth function is considered in the neighborhood of point x, the derivatives can be approximated using Taylor series expansions. This paper uses the central difference approximation since it is more accurate for smooth functions. Therefore, $\dot{\mathbf{X}}$ can be approximated by:

$$\dot{\mathbf{X}} \approx \frac{\mathbf{X}(i+1) - \mathbf{X}(i-1)}{2h} \tag{12}$$

where $\mathbf{X}(i)$ is the measured data at sample i and h is the sampling interval of the simulation or data collection process [24]. Fig. 3 depicts a comparison between the estimated derivatives of the IBR with the measured ones using central difference approximation technique with a sampling time of 50 microseconds. As it can be observed, the derivatives accurately match the actual derivatives of the states.

C. Sparse Identification of IBR Dynamics

If the IBR dynamics can be represented by a library of p candidate functions $\mathbf{\Theta}(\mathbf{X}, \mathbf{U}) \in \mathbb{R}^{n \times p}$(e.g., polynomials, or sinusoids), the vector of measured derivatives is a linear combination of columns from the candidate function library. The linear combination of columns is observed by the entries of matrix $\mathbf{\Xi} \in \mathbb{R}^{p \times n}$ such that [21]:

$$\dot{\mathbf{X}} = \mathbf{\Theta}(\mathbf{X}, \mathbf{U})\mathbf{\Xi}. \tag{13}$$

Having estimated $\dot{\mathbf{X}}$ from measurements, the library of candidate functions will be developed by including linear and nonlinear functions of the columns of $\mathbf{X}$ and $\mathbf{U}$. Typical candidate functions include polynomials and trigonometric functions for nonlinear systems, as shown in equation (14). In this equation, $\mathbf{P_i}(\mathbf{X}, \mathbf{U})$ denotes a nonlinear combination of i-order polynomials of $\mathbf{X}$ and $\mathbf{U}$. For example, $\mathbf{P_2}(\mathbf{X}, \mathbf{U})$

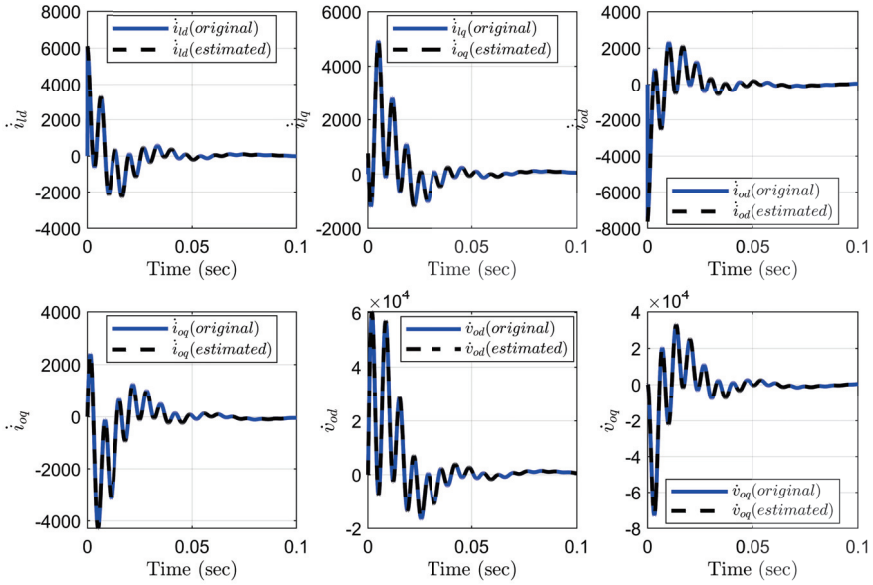

Figure. 3 Comparison between estimated derivatives and measured derivatives of the states for IBRs.

$$\Theta(\mathbf{X},\mathbf{U}) = \begin{bmatrix} | & | & | & | & | & & | & | & | & \\ 1 & \mathbf{X} & \mathbf{U} & \mathbf{P_2}(\mathbf{X},\mathbf{U}) & \mathbf{P_3}(\mathbf{X},\mathbf{U}) & \dots & \sin(\mathbf{X},\mathbf{U}) & \cos(\mathbf{X},\mathbf{U}) & \sin(\mathbf{2}(\mathbf{X},\mathbf{U})) & \dots \\ | & | & | & | & | & & | & | & | & \end{bmatrix} \tag{14}$$

includes polynomials up to second order such as $x_i x_j$, x_i^2, $x_i u_i$, and u_i^2. Having the estimated derivatives $\dot{\mathbf{X}}$ and $\boldsymbol{\Theta}(\mathbf{X},\mathbf{U})$, (13) can be solved to obtain a sparse matrix $\boldsymbol{\Xi}$ columns of which denote which candidate functions are active in the dynamics of the IBR. This process is normally solved iteratively using a sparse regression algorithm. The algorithm converges by solving an optimization of the form:

$$\boldsymbol{\xi}_h = \arg\min_{\hat{\boldsymbol{\xi}}_h} ||\dot{\mathbf{X}}_h - \boldsymbol{\Theta}(\mathbf{X},\mathbf{U})\hat{\boldsymbol{\xi}}_h||_2 + \lambda||\hat{\boldsymbol{\xi}}_h||_0 \tag{15}$$

where $\boldsymbol{\xi}_h$ is the h-th column of $\boldsymbol{\xi}$ represented by $\boldsymbol{\xi}_h = \begin{bmatrix}\xi_1 & \xi_2 & \dots & \xi_p\end{bmatrix}^T$ and $\dot{\mathbf{X}}_h$ represents the h-th column of $\dot{\mathbf{X}}$. The objective function in (15) has two components: the L2 norm $||.||_2$ that minimizes the error between the derivatives $\dot{\mathbf{X}}$ and estimated derivatives through an iterative least-squares problem and the L0 norm $||.||_0$ that minimizes the number of nonzero elements in $\boldsymbol{\xi}_h$ to promote sparsity in the coefficients matrix $\boldsymbol{\xi}$. It is noted that λ is the sparsity-promoting hyperparameter that is tuned imperially to result in the best estimation of the dynamics.

The minimization problem in (15) is solved using a sequentially thresholded least squares technique proposed in [25]:

$$S^k = \left\{j \in [p] : \left|\xi_j^k\right| \geq \lambda\right\}, \quad k \geq 0 \tag{16}$$

$$\hat{\boldsymbol{\xi}}_h^0 = \boldsymbol{\Theta}(\mathbf{X},\mathbf{U})^\dagger \dot{\mathbf{X}}_h \tag{17}$$

$$\boldsymbol{\xi}^{k+1} = \underset{\hat{\boldsymbol{\xi}}_h \in \mathbb{R}^p : \text{supp}(\boldsymbol{\xi}_h) \subseteq S^k}{\text{argmin}} \|\dot{\mathbf{X}}_h - \boldsymbol{\Theta}(\mathbf{X},\mathbf{U})\hat{\boldsymbol{\xi}}_h\|_2, \tag{18}$$

where k is the iteration number, $\boldsymbol{\Theta}(\mathbf{X},\mathbf{U})^\dagger$ is the pseudo-inverse of $\boldsymbol{\Theta}(\mathbf{X},\mathbf{U})$ and is defined as

$$\boldsymbol{\Theta}(\mathbf{X},\mathbf{U})^\dagger := [\boldsymbol{\Theta}(\mathbf{X},\mathbf{U})^T \boldsymbol{\Theta}(\mathbf{X},\mathbf{U})]^{-1} \boldsymbol{\Theta}(\mathbf{X},\mathbf{U})^T \tag{19}$$

and the support set of $\boldsymbol{\xi}_h$ is defined by $\text{supp}(\boldsymbol{\xi}_h) := \{j \in [p] : \xi_j \neq 0\}$. **Algorithm 1** explains the step-by-step procedure for obtaining the matrix $\boldsymbol{\Xi}$ using the sparse regression method. If the intent is to identify the signal $\mathbf{U}$ for feedback control, i.e., $\mathbf{U} = G(s)\mathbf{X}$, where $G(s)$ is the transfer function of the controller, the matrix of inputs can be identified using $\mathbf{U} = \boldsymbol{\Theta}_\mathbf{u}(\mathbf{X})\boldsymbol{\Xi}_\mathbf{u}$, where $\boldsymbol{\Theta}_\mathbf{u}(\mathbf{X})$ is the matrix of candidate functions with the terms corresponding to $\mathbf{U}$ have been removed from $\boldsymbol{\Theta}(\mathbf{X},\mathbf{U})$ and $\boldsymbol{\Xi}_\mathbf{u}$ can be found using the sparse regression algorithm similar to $\boldsymbol{\Xi}$.

IV. Case Studies

To validate the effectiveness of the proposed model-free IBR control in grid-tie mode, several case studies are carried out using time-domain simulations in MATLAB.

A. Training SINDy to Learn IBR Dynamics

First, the SINDy model is trained by perturbing the inputs of a simulated IBR model and capturing measurements. The measurements from states and inputs were utilized in **Algorithm 1** to obtain the matrix of sparse coefficients. For $\boldsymbol{\Theta}(\mathbf{X},\mathbf{U})$, the candidate terms include polynomials up to degree 2 and sinusoidal functions, i.e., u_i, x_i, $x_i x_j$, x_i^2, $x_i \cos x_j$, $x_i \sin x_j$, $u_i \cos x_j$, $u_i \sin x_j$. The identified

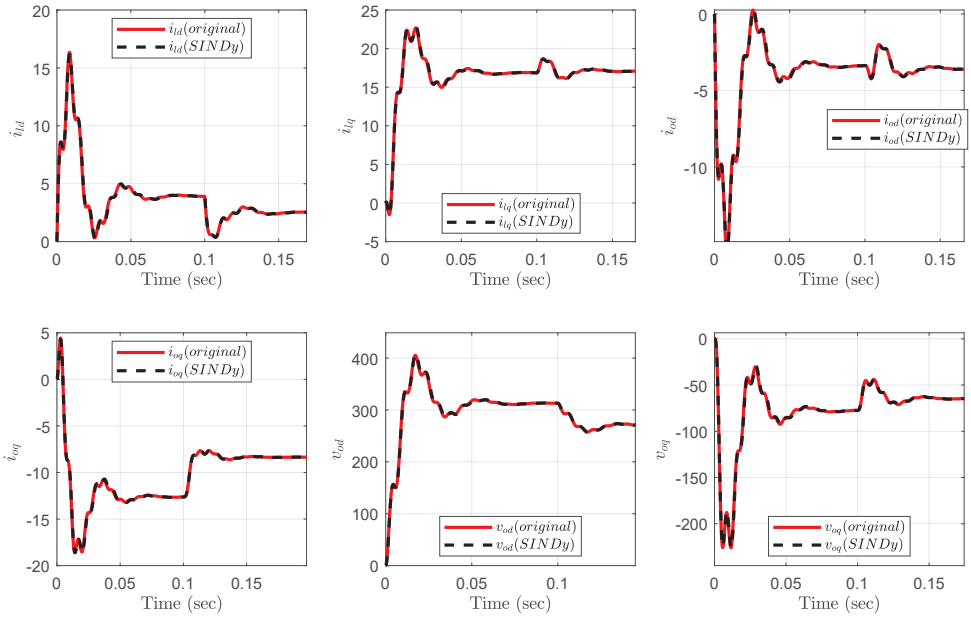

Figure. 4 Training of SINDy to learn the dynamics of IBR.

Algorithm 1 Sparse Regression Algorithm

Input: Measurements $\mathbf{X}, \mathbf{U}$
Input: Estimated derivatives$\dot{\mathbf{X}}$

procedure STLS
$\Gamma = \Theta \backslash \dot{\mathbf{X}}$ (least-square solution)
  for k $= 1:10$ **do** (number of iterations)
    Set λ (sparcification knob)
    $|\Xi| < \lambda \longrightarrow ind_{small}$
    $\Xi(ind_{small}) \longrightarrow 0$
    for k $= 1:$ n **do** (n dimension of state $\mathbf{X}$)
      $ind_{big} \neq ind_{small}(:,k)$
      $\Xi(ind_{big},k) = \Theta(:,ind_{big}) \backslash \dot{\mathbf{X}}(:,k)$
    end for
  end for

Output: sparse matrix Ξ

coefficients $\boldsymbol{\Xi}$ for the studied IBR model were used to develop a data-driven model in MATLAB. A comparison between the physical model and the identified model is shown in Figure. 4. This data-driven IBR model accurately reflects the dynamics of the physical model, as can be seen.

B. IBR's Active and Reactive Power Control using Data-Driven Model

In the second case, the control architecture shown in Fig. 2 was implemented on the data-driven model and then was applied to the simulated IBR using the parameters provided in [23]. The PI control gains for the data-driven model include $k_{ip} = 0.11$ and $k_{ii} = 11$ whereas for the physical systems with actual dynamics, these gains were calculated to be $k_{ip} = 0.1$ and $k_{ii} = 10$. Simulation results for the states are illustrated in Fig. 5 and the active and reactive power tracking results are shown in Fig. 6. It is noted that the results of the proposed data-driven control design accurately match with the physics-based design.

V. Conclusion

In this paper, a model-free identification of IBR dynamics for control purposes was studied. Using sparse identification of nonlinear dynamics with control along with available measurements, dynamics of the IBRs were predicted utilizing a library of candidate functions from measurement basis. The learned dynamics were then used to design a controller that can regulate the converter current and provide active/reactive power control capabilities in grid-tie mode of operation. It was demonstrated that sparse identification can accurately identify the IBR dynamics with limited measurement data (0.15 seconds with 50 microseconds sampling time) and the data-driven control design can provide accurate active and reactive power control as a physics-based control design. Such data-driven control framework can significantly reduce the existing complexities of control design in modern power systems. Future research will focus on hardware validation of the proposed data-driven control in a three-phase voltage source converter.

References

[1] S. M. Ho, A. Lomi, E. C. Okoroigwe, and L. R. Urrego, "Investigation of solar energy: The case study in malaysia, indonesia, colombia and nigeria," *International Journal of Renewable Energy Research*, vol. 9, no. 1, 2019.

[2] K. Kumar, N. R. Babu, and K. Prabhu, "Design and analysis of an integrated cuk-sepic converter with mppt for standalone wind/pv hybrid system," *International Journal of Renewable Energy Research (IJRER)*, vol. 7, no. 1, pp. 96–106, 2017.

[3] K. Anwar and S. Deshmukh, "Assessment and mapping of solar energy potential using artificial neural network and gis technology in the southern part of india," *International Journal of Renewable Energy Research (IJRER)*, vol. 8, no. 2, pp. 974–985, 2018.

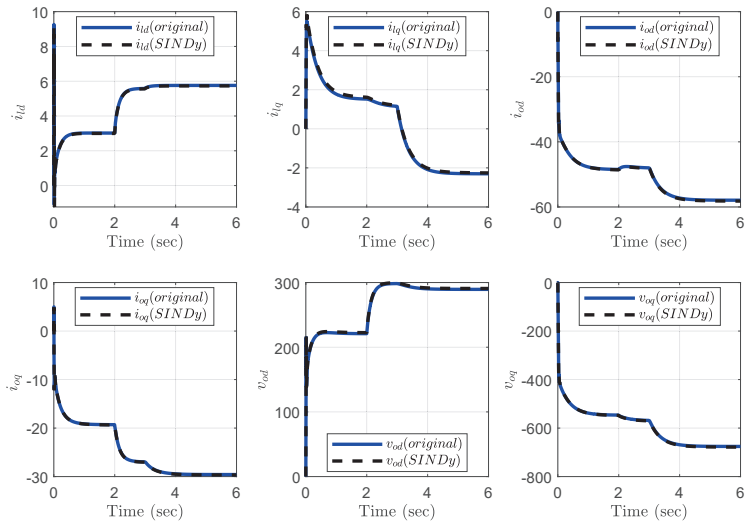

Figure. 5 Trajectory of states for active and reactive power control.

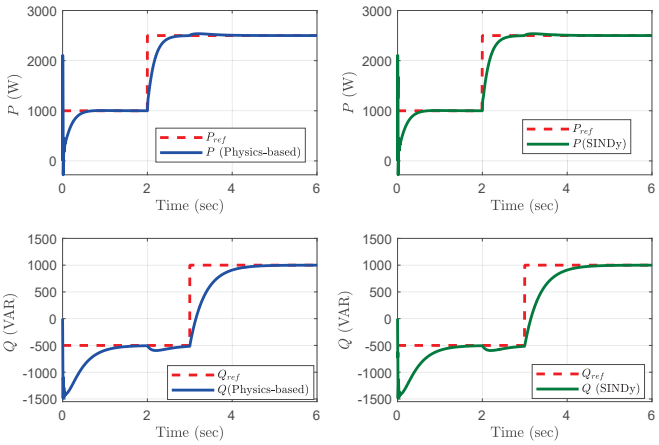

Figure. 6 Active and reactive power measurements.

[4] Y. Althuwaini and S. P. Philbin, "Techno-economic analysis of solar power plants in kuwait: Modelling the performance of pv and csp systems," *International Journal of Renewable Energy Research (IJRER)*, vol. 11, no. 4, pp. 2009–2024, 2021.

[5] V. Suresh and S. Sreejith, "Power flow analysis incorporating renewable energy sources and facts devices," *International Journal of Renewable Energy Research (IJRER)*, vol. 7, no. 1, 2017.

[6] T. Tawfik, M. Badr, O. Abdellatif, H. Zakaria, and M. EL-Bayoumi, "Techno-enviro-economic evaluation for hybrid energy system considering demand side management," *International Journal of Renewable Energy Research (IJRER)*, vol. 12, no. 2, pp. 623–635, 2022.

[7] M. Liu, L. Tan, and S. Cao, "Method of dynamic mode decomposition and reconstruction with application to a three-stage multiphase pump," *Energy*, vol. 208, p. 118343, 2020.

[8] H. Lu and D. M. Tartakovsky, "Prediction accuracy of dynamic mode decomposition," *SIAM Journal on Scientific Computing*, vol. 42, no. 3, pp. A1639–A1662, 2020.

[9] T. Qin, K. Wu, and D. Xiu, "Data driven governing equations approximation using deep neural networks," *Journal of Computational Physics*, vol. 395, pp. 620–635, 2019.

[10] M. Raissi, P. Perdikaris, and G. E. Karniadakis, "Multistep neural networks for data-driven discovery of nonlinear dynamical systems," *arXiv preprint arXiv:1801.01236*, 2018.

[11] M. Al-Gabalawy, "Deep learning for koopman operator optimal control," *ISA transactions*, 2021.

[12] A. Mauroy, I. Mezić, and Y. Susuki, *The Koopman Operator in Systems and Control: Concepts, Methodologies, and Applications*. Springer Nature, 2020, vol. 484.

[13] S. L. Brunton, J. L. Proctor, and J. N. Kutz, "Discovering governing equations from data by sparse identification of nonlinear dynamical systems," *Proceedings of the National Academy of Sciences*, vol. 113, no. 15, pp. 3932–3937, 2016.

[14] U. Fasel, E. Kaiser, J. N. Kutz, B. W. Brunton, and S. L. Brunton, "Sindy with control: A tutorial," *arXiv preprint arXiv:2108.13404*, 2021.

[15] G. Kandaperumal, K. P. Schneider, and A. K. Srivastava, "A data-driven algorithm for enabling delay tolerance in resilient microgrid controls using dynamic mode decomposition," *IEEE Transactions on Smart Grid*, vol. 13, no. 4, pp. 2500–2510, 2022.

[16] J. Bedi and D. Toshniwal, "Empirical mode decomposition based deep learning for electricity demand forecasting," *IEEE access*, vol. 6, pp. 49 144–49 156, 2018.

[17] M. Netto and L. Mili, "A robust data-driven koopman kalman filter for power systems dynamic state estimation," *IEEE Transactions on Power Systems*, vol. 33, no. 6, pp. 7228–7237, 2018.

[18] Y. Hirase, Y. Ohara, N. Matsuura, and T. Yamazaki, "Dynamics analysis using koopman mode decomposition of a microgrid including virtual synchronous generator-based inverters," *Energies*, vol. 14, no. 15, p. 4581, 2021.

[19] K. A. Severson, P. M. Attia, N. Jin, N. Perkins, B. Jiang, Z. Yang, M. H. Chen, M. Aykol, P. K. Herring, D. Fraggedakis *et al.*, "Data-driven prediction of battery cycle life before capacity degradation," *Nature Energy*, vol. 4, no. 5, pp. 383–391, 2019.

[20] Y. Li, Y. Liao, X. Wang, L. Nordström, P. Mittal, M. Chen, and H. V. Poor, "Neural network models and transfer learning for impedance modeling of grid-tied inverters," in *2022 IEEE 13th International Symposium on Power Electronics for Distributed Generation Systems (PEDG)*. IEEE, 2022, pp. 1–6.

[21] S. L. Brunton, J. L. Proctor, and J. N. Kutz, "Discovering governing equations from data by sparse identification of nonlinear dynamical systems," *Proceedings of the national academy of sciences*, vol. 113, no. 15, pp. 3932–3937, 2016.

[22] ——, "Sparse identification of nonlinear dynamics with control (sindyc)," *IFAC-PapersOnLine*, vol. 49, no. 18, pp. 710–715, 2016.

[23] A. Yazdani and R. Iravani, *Voltage-sourced converters in power systems: modeling, control, and applications*. John Wiley & Sons, 2010.

[24] S. Larsson and V. Thomée, *Partial differential equations with numerical methods*. Springer, 2003, vol. 45.

[25] L. Zhang and H. Schaeffer, "On the convergence of the sindy algorithm," *Multiscale Modeling & Simulation*, vol. 17, no. 3, pp. 948–972, 2019.